Geometry dependence of the acoustic transmission and reflection properties of centrifugal pumps based on an internal lumped parameter model

Guidong Li [(a)], Manuel García-Díaz [(a)], Guillermo Laine [(a)] and Jorge Parrondo [(a)]*

[(a)] Department of Energy, University of Oviedo. E-33204 Gijón, Spain

* Corresponding author: parrondo@uniovi.es

Abstract

As a tool to characterize the acoustic properties of conventional centrifugal pumps, consisting in impeller and vaneless volute casing, a new acoustic lumped parameter model has been developed that simulates the acoustic field induced inside the pumps when subject to low-frequency sound sources. The model is based on a network of nodes distributed through the pump, with local transfer matrices connecting pairs of nodes at neighboring regions, and so it is referred to as an internal transfer matrix model. At the present stage the model has been implemented in a procedure to determine the pump passive acoustic properties, either in terms of a transmission matrix or a scattering matrix, though in a future step the model is to be applied for the characterization of the internal sound sources in centrifugal machinery. This paper presents the assumptions of the model and the resolution approach to calculate transmission or scattering matrices, as well as a summary of results for a reference pump that shows the sensitivity of predictions with respect to several geometrical pump parameters. Finally, a contrast is carried out between experimental data recently reported in the literature on the scattering matrices for five pumps of different geometry and the corresponding predictions obtained from i) the new lumped parameter model based on internal transfer matrices and ii) a classical pump model based on an electrical system analogy. The results show that the predictions of the new transfer matrix model are always in reasonable quantitative agreement with measurements, and that, as frequency is increased, its prediction capability clearly outperforms that of the electrical analogy model regardless the pump specific speed or the geometrical features.

Keywords

Centrifugal pump, Low frequency sound, Lumped parameter model, Scattering matrix, Geometry dependence.

1. Introduction

Hydraulic systems with fluid machinery usually exhibit fluid-dynamic pulsations that can be transmitted to distant components along the piping and have potential to induce high noise and vibration levels [1-4]. Common pulsation sources are the pumps themselves [5-7]. Even in the absence of cavitation or other abnormal conditions, pumps behave as discrete low frequency acoustic sources that radiate sound to the suction and discharge ducts, as well as air-borne sound from the pump casing and pipes [7, 8]. In the case of centrifugal pumps with vaneless volute, the most common ones, significant excitation can be expected at the blade-passing frequency and harmonics even when operating at the design flow-rate, because the non-uniform flow that exits the impeller is perceived as intermittent at the volute and in particular at the tongue [5, 9]. At off-design conditions the magnitude of that blade-passing excitation can increase remarkably [10, 11], while other phenomena with different characteristic frequencies may appear, such as rotating stall [8, 12]. However, the pressure fluctuations induced at a given frequency and position along the pipes also depend on the acoustic response of the system, i.e., on how the acoustic pulsations are transmitted or reflected at each element of the system [3, 4, 13, 14]. That includes the pump itself [2, 15].

Especially during the last decade there has been a considerable increasing interest in analyzing and quantifying the internal sound sources in centrifugal fans and pumps by means of computational simulations that assume Lighthill's acoustic analogy [7]. This implies three steps: *i*) the CFD calculation of the unsteady flow, which can include dynamic boundary conditions to account for the impedance of the connected pipes [16]; *ii*) the assignment of acoustic sources, usually as dipoles related to the pressure fluctuations on walls [11, 13, 17, 18]; and *iii*) the computation of the sound field, usually by a finite element or a boundary element method [11, 17-20]. Several recent studies were aimed to evaluate the effect of different geometrical parameters of some specific pumps on the sound generated, including the impeller outlet width [21, 22], the blade outlet angle [23, 24], the number of blades [25] or even a combination of parameters [26].

However, the predictions so obtained are very sensitive to the details of the computational mesh and the turbulence model, especially when the pump operates at off-design conditions, and experimental contrast is always necessary. To characterize pumps or other fluid machinery as sources that radiate sound to the connected pipes, the usual

experimental procedures require a previous characterization of the transmission and reflection properties of the machine [2, 27, 28]. In the case of pumping systems, the frequencies of interest are usually low enough for the wave-lengths to be at least one order of magnitude greater than the diameters of piping or pump impeller, so that effective acoustic propagation is restricted to the plane wave mode. Because of that, the passive acoustic properties of a pump can be condensed in a transmission matrix **T** [4, 29] that relates linearly two acoustic variables, e.g. the acoustic pressure p and the acoustic mass velocity v, at the suction and discharge ports of the pump when there is no internal sound generation at the frequency of interest:

$$\begin{bmatrix} p_S \\ v_S \end{bmatrix} = \mathbf{T} \begin{bmatrix} p_D \\ v_D \end{bmatrix} = \begin{bmatrix} T_{11} & T_{12} \\ T_{21} & T_{22} \end{bmatrix} \begin{bmatrix} p_D \\ v_D \end{bmatrix} \tag{1}$$

Another convenient formulation often used to describe the passive acoustic properties of two-port elements can be obtained by choosing the incoming and exiting pressure waves as the state variables at each port [4, 27] (Fig. 1). Considering again the pump as a purely passive element, this formulation allows to express the exiting pressure waves from the pump ports as a linear function of the entering pressure waves, through the so-called scattering matrix **S**:

$$\begin{bmatrix} p_S^- \\ p_D^+ \end{bmatrix} = \mathbf{S} \begin{bmatrix} p_S^+ \\ p_D^- \end{bmatrix} = \begin{bmatrix} S_{11} & S_{21} \\ S_{12} & S_{22} \end{bmatrix} \begin{bmatrix} p_S^+ \\ p_D^- \end{bmatrix} \tag{2}$$

where superscripts '+' and '-' represent propagation in the positive (streamwise) and negative direction respectively, and:

$$\begin{cases} p_S = p_S^+ + p_S^- \\ p_D = p_D^+ + p_D^- \end{cases} \tag{3}$$

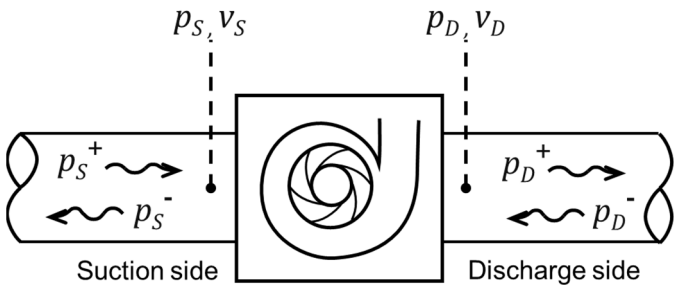

Fig. 1. Incoming and exiting pressure waves at the pump ports.

The transmission matrix and the scattering matrix are interrelated, so that the elements of **T** can be obtained from the elements of **S** and vice versa [2, 30] (see Eq. 21).

In order to estimate the transmission matrix, Stirnemann et al. [29] used an electrical analogy to represent the pump as a series impedance Z_2, which connects the suction and discharge ports of the pump, plus two parallel admittances, Y_1 and Y_3, one at each port (Fig. 2).

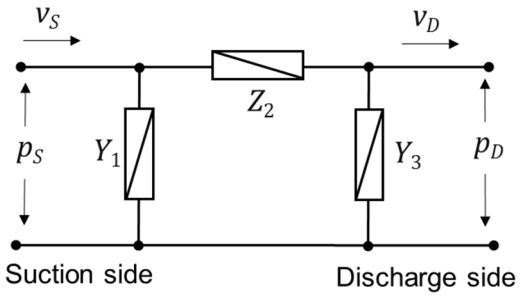

Fig. 2. Electrical analogy for pumps [29].

According to that analogy, the transmission matrix **T** results to be:

$$\mathbf{T} = \begin{bmatrix} 1 + Z_2\, Y_3 & Z_2 \\ Y_1 + Y_3 + Y_1\, Z_2\, Y_3 & 1 + Z_2\, Y_1 \end{bmatrix} \tag{4}$$

Equation (4) gained some general use though the choice for the equivalent electrical parameters was not clear and varied among researchers. Rzentkowski and Zbroja [2, 15] suggested the following estimates for Y_1, Z_2 and Y_3:

$$\begin{cases} Z_2 = -g\dfrac{\partial H}{\partial Q} + i \cdot \omega \dfrac{V_{IMP}}{A_P^2} \\ Y_1 = Y_3 = i \cdot \omega \dfrac{V_{PUMP}}{2c^2} \end{cases} \tag{5}$$

where $\partial H/\partial Q$ represents the slope of the pump characteristic curve, V_{IMP} and V_{PUMP} are the volumes of the impeller and pump respectively and A_P is the average of the pump eye section and the throat section. However, they only recommended the application of that model for a low range of frequency. In general the order of magnitude of the entries T_{11} and T_{22} is 1, T_{12} is very large and T_{21} is very low. Despite this, Bardeleben and Weaver [30], who conducted extensive tests on a laboratory pump, remarked the importance of not neglecting the entry T_{21} in order to improve the predictions of the scattering matrix.

However, their experimental data exhibited a large dispersion and the study was not conclusive.

Indeed, obtaining reliable experimental data for the transmission or scattering matrices of pumps has proved to be a difficult task, due to the distorting effects of the pump induced noise, flow turbulence and pipe vibration. They can be partially circumvented by taking measurements with redundant sensors [30-33], but even at pump-off conditions the results can be affected by trapped air bubbles or casing compliance [28,30]. Probably the most complete and reliable set of experimental data on pump scattering matrices is the one recently reported by Lehr et al. [34] and Brümmer et al. [35], who tested a group of pumps with different features and non-dimensional specific speed ω_S ranging from 0.46 to 0.99.

Parrondo et al. [36] proposed an alternative approach to characterize the acoustic transmission properties and the internal sound generation sources of centrifugal pumps, which was based on combining a simple acoustic model with pressure fluctuation measurements on the pump volute. The acoustic model was designed to reproduce the internal sound field radiated from arbitrary ideal harmonic sources, by considering multiple sound circulations along the volute and partial reflections at the throttle while continuously exchanging sound with the impeller channels. That acoustic model was implemented in a hill-climbing algorithm that progressively varied the properties of the ideal sound sources until identifying the set of sources whose predictions best reproduced the available experimental data based on a least square error criterion. Keller et al. [13] applied that procedure on a test pump for different operating points, resulting in the identification of two ideal sources located in the tongue region of the volute: for flow-rates below nominal they were two monopoles that behaved as a dipole, whereas for nominal and higher flow rates they were two dipoles that resembled a linear quadrupole.

Under the perspective of a strategy similar to that of references [13, 36], this paper presents a novel acoustic model aimed to determine the internal sound distribution in centrifugal pumps under the presence of internal or external sources. The model is based on a special network of internal nodes and local frequency dependent transfer matrices that relate the acoustic variables of nearby nodes. Compared to the sound recirculation model of [36], the new model is not restricted to anechoic suction, it is not subject to convergence issues and, overall, allows for much shorter calculation times. The latter is

of particular interest because, in a future step, the model is expected to be repeatedly used in an iterative hill-climbing procedure analogous to [13] in order to quantify the properties of the sound sources that best reproduce the pressure fluctuation measurements available for a given pump, as a means to analyze the excitation mechanisms depending on the operating point. Prior to that objective, the scope of the present work has focused on the application of the new model to determine the transmission matrix and the scattering matrix of a given pump as a function of frequency, by imposing auxiliary sources at the suction and discharge ports.

This paper exposes the assumptions of the new model, the resolution approach to calculate transmission or scattering matrices and the effect of several model parameters on the predictions for a test pump. Finally, a contrast is performed between the scattering matrix data reported by Brümmer et al. [34, 35] for five different pumps and the corresponding predictions obtained from the new transfer matrix model as well as from Stirnemann et al´s electrical analogy [29].

2. Acoustic Model

This research focuses on conventional centrifugal pumps with a shrouded impeller that can rotate in a vaneless volute casing (Fig. 3). The impeller takes the fluid in the axial direction from the suction port of the pump and drives it to the radial direction through passage channels defined by blades and shrouds. Around the impeller, the exiting fluid is collected by the volute, which has an increasing cross-section from a minimum (at tongue) until the throat. Then flow continues along a curved diffuser, until the discharge port of the pump.

There is substantial evidence from a number of previous experimental studies that the passive acoustic properties at low frequency noise for non-cavitating centrifugal pumps are little affected by the operating point [30] or the rotation speed, up to the point of advising to conduct tests with pumps off [28, 31, 32]. Hence, for the present study it was considered a non-rotating impeller with no flow across the pump.

For this pump model, the volute casing is represented as a chamber that is short in the axial direction, with most of the central part being occupied by the impeller. In that

chamber, sound is assumed to propagate in plane wave mode along the volute (i.e. in the circumferential direction), while receiving and transmitting sound to the impeller channels. The exit of each impeller channel plus the throttle are considered as side ports of the volute chamber, allocated along the circular direction. The model assumes that the internal sound field can be reasonably described by establishing a network with a few nodes and transfer matrices that connect nodes of neighboring regions. In particular, the sound exchange between impeller channels and volute is assumed to take place only at one specific location or region for each impeller channel.

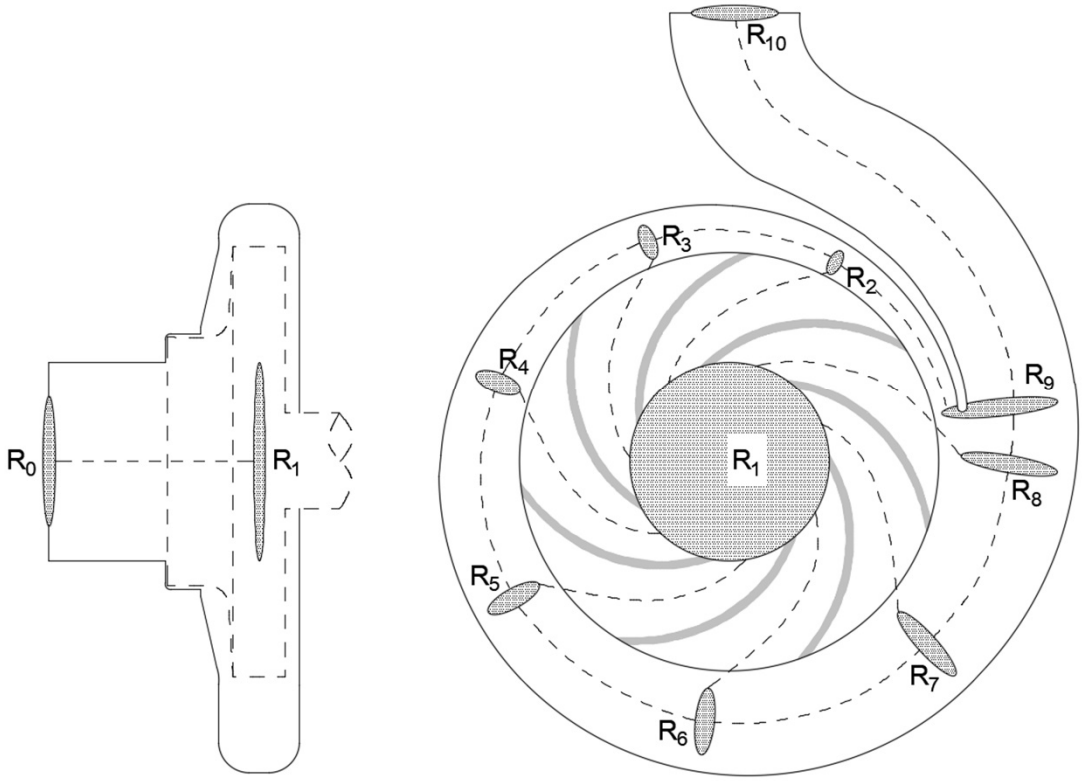

Fig. 3. Pump reference regions to characterize the internal sound transmission.

The regions considered inside the pump are (Fig. 3): pump inlet, impeller eye, volute sections next to the exit of each impeller channel, tongue-throttle zone and pump outlet. For instance, a pump with a 7-blade impeller would have 11 regions, labelled R_0 to R_{10} in Fig. 3. In case of assuming internal sound sources in the pump, another region should be assigned to each of them. The latter, however, is beyond the scope of this study, since at present the purpose is to check the capability of the model to estimate the passive acoustic

properties in terms of transmission or scattering matrices. In consequence any sound source shall be external and sound is assumed to enter the pump only through the suction and discharge ports.

In this system, each region R_i contains one or more nodes n_{im}, which are positions with some local value of acoustic pressure p_{im} and acoustic mass flow velocity v_{im}. In particular, each region contains one node for every other connected region, as follows:

- Pump inlet region (R_0 in Fig. 3*)*: one single node n_{00}, facing the impeller eye.
- Impeller eye region (R_1): one central node n_{10} facing the pump inlet, plus another z_B nodes, each at the inlet of an impeller channel (Fig. 4(a)).
- Regions along the volute: one node at the outlet of the corresponding impeller channel plus two other nodes facing the previous and subsequent volute regions (Fig. 4(b)).
- Tongue-throttle region (R_9 in Fig. 3): it has three nodes as well, two of them at both sides of the impeller-tongue gap facing the volute neighboring regions and the third one at the pump throttle facing the impeller outlet region (Fig. 4(c)).
- Pump outlet region (R_{10}): one single node (n_{100} for z_B =7) facing the throttle.

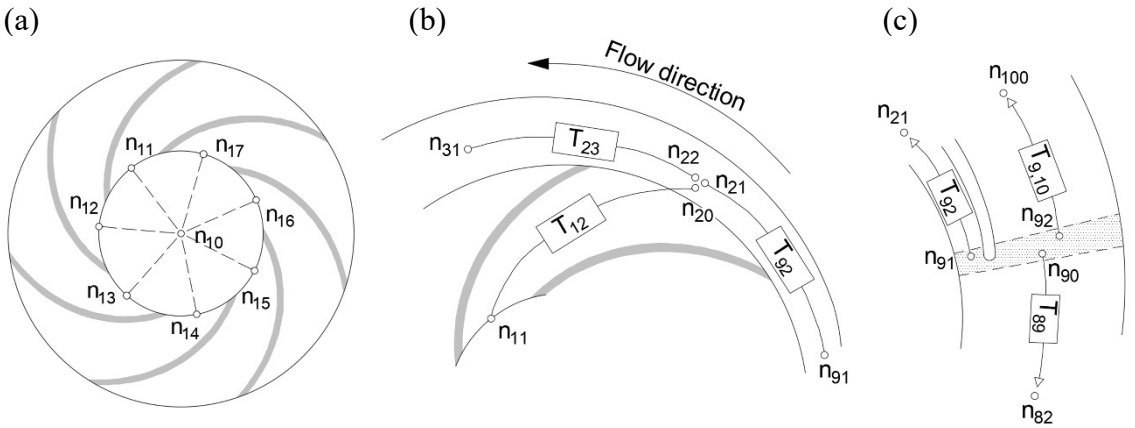

Fig. 4. Nodes at the impeller eye region (a), volute region (b) and tongue region (c).

Together, there would be 34 nodes for a pump with z_B= 7 blades, like the one shown in Fig. 3. The acoustic pressure p_{im} and mass flow velocity v_{im} at the nodes n_{im} of any internal region R_i are considered to verify:

- Uniform acoustic pressure:

$$p_{i0} = p_{i1} = \cdots = p_{im} \tag{6}$$

- Mass flow continuity:

$$\sum_m v_{im} = 0 \tag{7}$$

In the case of the pump inlet and outlet regions, special boundary conditions are to be imposed depending on the external acoustic load applied on the pump.

Every node n_{im} in the domain, located in region R_i, must be connected to another node n_{jn} of a neighboring region R_j by means of a specific transfer matrix $\mathbf{T_{ij}}$ so that:

$$\begin{bmatrix} p_{im} \\ v_{im} \end{bmatrix} = \mathbf{T_{ij}} \begin{bmatrix} p_{jn} \\ v_{jn} \end{bmatrix} = \begin{bmatrix} T_{ij11} & T_{ij12} \\ T_{ij21} & T_{ij22} \end{bmatrix} \begin{bmatrix} p_{jn} \\ v_{jn} \end{bmatrix} \tag{8}$$

In order to determine these transfer matrices, it was assumed that the respective sound paths between connected nodes are equivalent to ducts with a cross-section that varies linearly from one end to the other. Each transfer matrix was calculated by means of a segmentation method with the *matrizant* approach [37], which consists in (Fig. 5):

- i) divide each duct in N thin slices,
- ii) assign the transfer matrix to each slice as would correspond to an exponentially shaped duct with appropriate values of cross-section at the two sides depending on the slice position, and
- iii) multiply sequentially the transfer matrices of the N slices.

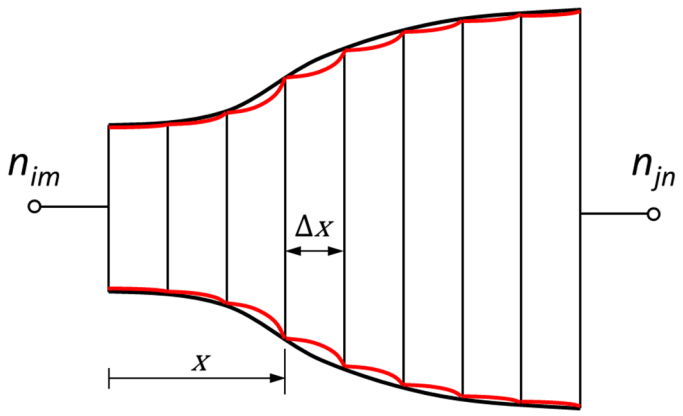

Fig. 5. Passage between two nodes n_{im} and n_{jn} as a succession of slices with cross-section varying exponentially.

For a slice of thickness Δx that starts at the longitudinal coordinate x and has an exponential shape between the known cross-sections $A(x)$ and $A(x+\Delta x)$, the transfer matrix can be defined as [38]:

$$\begin{bmatrix} p_x \\ v_x \end{bmatrix} = \mathbf{T}_{\boldsymbol{S}(x)} \begin{bmatrix} p_{x+\Delta x} \\ v_{x+\Delta x} \end{bmatrix} = \\ = \begin{bmatrix} e^{h\Delta x}\left(\cos\alpha - \frac{s}{k'}\sin\alpha\right) & j\, y_0\, e^{-h\Delta x}\, \frac{k_0}{k'}\sin\alpha \\ \frac{j}{y_0}\, e^{h\Delta x}\, \frac{k_0}{k'}\sin\alpha & e^{-h\Delta x}\left(\cos\alpha + \frac{s}{k'}\sin\alpha\right) \end{bmatrix} \begin{bmatrix} p_{x+\Delta x} \\ v_{x+\Delta x} \end{bmatrix} \quad (9)$$

where k_0 is the wave number at position x, $y_0 = c/A(x)$ is the characteristic impedance and:

$$h = \frac{1}{\Delta x}\ln\frac{A(x+\Delta x)}{A(x)} \quad (10)$$

$$k' = \sqrt{k_0^2 - h^2} \quad (11)$$

$$\alpha = k'\Delta x \quad (12)$$

In consequence, the transfer matrix $\mathbf{T}_{\boldsymbol{ij}}$ between the nodes that connect regions R_i and R_j is calculated as:

$$\mathbf{T}_{\boldsymbol{ij}} = \prod_{k=1}^{N} \mathbf{T}_{\boldsymbol{S}(x_k)} = \prod_{k=1}^{N} \mathbf{T}_{\boldsymbol{S}(k\cdot\Delta x)} \quad (13)$$

Some other special considerations were taken into account as follows:

i) End corrections were included for the transfer matrices that represent the impeller channels (both sides) and also the pump diffuser (only throttle side), by adding short pipes with equivalent lengths of 60% of the associated hydraulic radius [38].

ii) At the outlet of the impeller channels, sound is considered to expand abruptly to a cross-surface that covers an arc of a cylinder with the radius of the impeller outlet, the axial width of the volute and a peripheral extension that is proportional to that of the impeller channel by a factor $k_P \geq 1$ (Fig. 6(a)). Once in the volute, those curved sound waves are assumed to progress in the direction β_2 of the impeller blades (Fig. 6(a)) up to a medium position M between impeller and volute surface (Fig. 6(b)). A new transfer matrix was determined for that short path across a fraction of the volute by means of the segmentation method described

above. Then the previous transfer matrix of each impeller channel was multiplied by that new matrix.

iii) The transition between the exit area of the impeller channels (β_2 direction) and the volute (peripheral direction) is affected by sound reflection from the volute wall, in a fashion comparable to an extended-tube resonator of the reversal type (Fig. 6(b)). In order to take this effect into account, the transfer matrix of each impeller channel was multiplied by the matrix of a lumped shunt element [38], as defined in Eq. (14):

$$\mathbf{T_{Sh}} = \begin{bmatrix} 1 & 0 \\ 1/Z_R & 1 \end{bmatrix} \tag{14}$$

In Eq. (14), Z_R represents the impedance of a branch resonator. If $\mathbf{T_R}$ is the transfer matrix associated to the radial path between the central position in the volute (*M* in Fig. 6(b)) and the volute internal surface, which can be estimated by using the segmentation method again, the corresponding resonator impedance Z_R results to be:

$$Z_R = \frac{T_{R11}}{T_{R21}} \tag{15}$$

iv) Subsequent sound propagation along the volute also covers the lateral cavities between impeller and casing, assuming that both front and rear casing surfaces are flat and perpendicular to the axis (Fig. 6(b)), with radial extensions from the impeller inlet seal and the shaft ring respectively up to the volute.

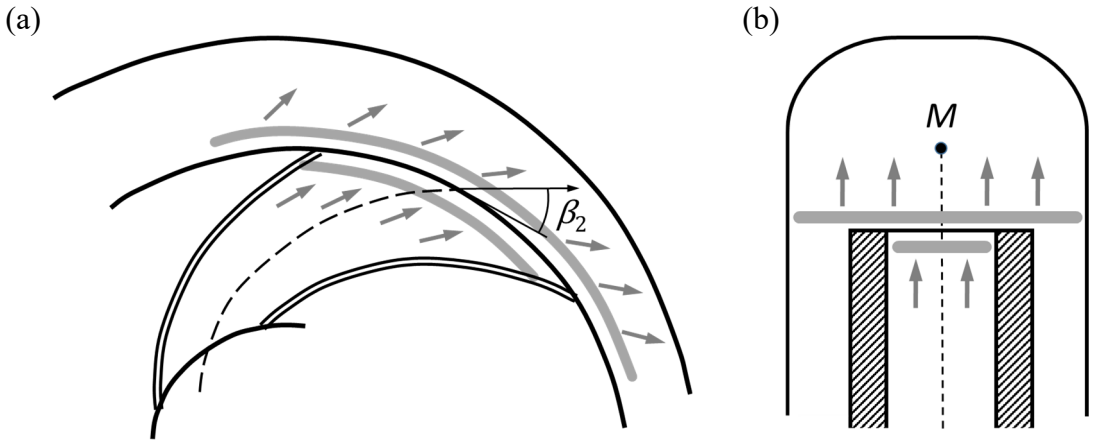

Fig. 6. Transition from an impeller channel to volute: a) frontal view; b) meridional view.

The transfer matrices that relate nodes along the volute depend on the local cross-section and so they are different for every pair of connected nodes. Moreover, they depend somewhat on the relative position of the impeller with respect to the tongue, as the latter determines the precise position of all the nodes in the volute. A similar dependence occurs for the transfer matrices of the impeller channels, because the transition effects from impeller to volute depend too on the magnitude of the volute cross-section.

3. System resolution

In the acoustic model for centrifugal pumps described above, the acoustic pressure and mass velocity at all the nodes in the system constitute a finite number of unknown complex variables. They are to be determined according to the relationships established for the nodes in a given region (Eqs. 6 and 7) and by the transfer matrices between nodes of neighboring regions.

The number of nodes depends on z_B, the number of blades of the impeller, and so does the number of variables and equations. For the case of z_B=7 (Fig. 7) there are 34 nodes, i.e. 68 unknowns. Besides there are 17 transfer matrices each producing 2 equations, plus 23 pressure identity equations and 9 continuity equations by virtue of Eqs. (6) and (7) respectively. This makes a total of 66 linear equations and hence two more equations are needed to obtain a closed system. These two additional equations correspond to boundary conditions at the suction and discharge ports of the pump, which, for z_B=7, are represented by nodes $n_S = n_{00}$ and $n_D = n_{100}$ respectively (Fig. 7). And those boundary conditions depend on the external acoustic load applied on the pump.

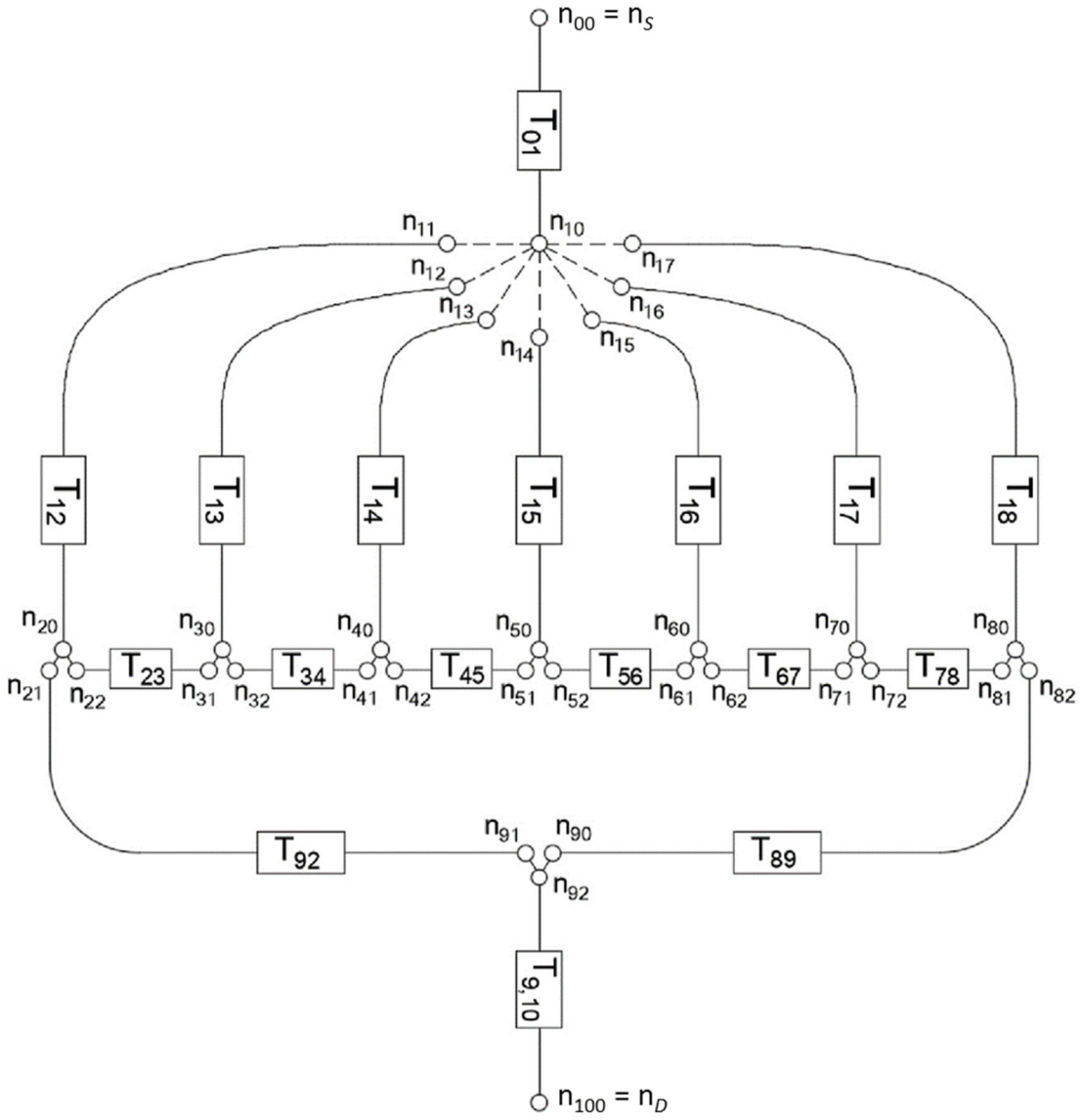

Fig. 7. Network of nodes and transfer matrices for a pump with a seven-blade impeller.

In order to determine the overall transmission matrix of a given pump, it is necessary to consider two situations with independent acoustic loads, hence with independent sets of boundary conditions. A convenient choice is summarized in Table 1. Once the system of equations is closed it can be solved by any method suitable for linear equation systems [39]. Direct methods are preferable since the expected number of variables and equations is low (68 complex unknowns and equations for z_B=7 blades). For the calculations reported below the classical method of Gaussian elimination proved to be very effective when used with complete pivoting during the process.

Table 1. Acoustic loads and boundary conditions to determine the pump transmission matrix. *S*=node at suction port (n_S=n_{00} in Fig. 7); *D*=node at discharge port (n_D=n_{100} in Fig. 7).

Load	Boundary condition	Description	Equation	
I	BC-*I*-1	External source at suction pipe, inducing an incoming unitary pressure wave.	$p_S + y_S\, v_S = 2$	(16)
	BC-*I*-2	Discharge piping with anechoic end.	$p_D - y_D\, v_D = 0$	(17)
II	BC-*II*-1	Suction piping with anechoic end.	$p_S + y_S\, v_S = 0$	(18)
	BC-*II*-2	External source at discharge pipe, inducing an incoming unitary pressure wave.	$p_D - y_D\, v_D = 2$	(19)

The application of the whole procedure to form and solve the equation system results in the values of all the unknown variables, for each of the two acoustic loads considered. In particular, the overall transmission matrix of the pump **T** has to relate the acoustic pressure and mass velocity at the suction and discharge ports of the pump, i.e. at nodes n_S and n_D (Fig. 7), so that for both acoustic loads *I* and *II* it must be verified:

$$\begin{bmatrix} p_S \\ v_S \end{bmatrix}_{I-II} = \mathbf{T} \begin{bmatrix} p_D \\ v_D \end{bmatrix}_{I-II} = \begin{bmatrix} T_{11} & T_{12} \\ T_{21} & T_{22} \end{bmatrix} \begin{bmatrix} p_D \\ v_D \end{bmatrix}_{I-II} \tag{20}$$

Eq. (20) constitutes two pairs of equations, with each pair involving only the two entries of either the first or the second row of **T**. In consequence all the elements of **T** can be obtained easily.

Finally, the scattering matrix of the pump, **S**, can also be obtained from the elements of the transmission matrix, by using the following relationships [30]:

$$\begin{cases} S_{11} = \dfrac{1}{Den}\left(T_{11} - y_S\, T_{21} + \dfrac{T_{12}}{y_D} - \dfrac{y_S\, T_{22}}{y_D}\right) \\ S_{12} = \dfrac{2}{Den} \\ S_{21} = \dfrac{2}{Den}\left(T_{11}\, T_{22} - T_{12}\, T_{21}\right) \\ S_{22} = \dfrac{1}{Den}\left(-T_{11} - y_S\, T_{21} + \dfrac{T_{12}}{y_D} + \dfrac{y_S\, T_{22}}{y_D}\right) \\ Den = T_{11} + y_S\, T_{21} + \dfrac{T_{12}}{y_D} + \dfrac{y_S\, T_{22}}{y_D} \end{cases} \tag{21}$$

No acoustic dissipation has been included in the internal transfer matrices, as well as no effect of fluid velocity on the effective sound speed. In consequence the elements T_{11} and T_{22} of the pump transmission matrix only have real part, the elements T_{12} and T_{21} only have imaginary part and the determinant of **T** is equal to 1 (real part only), as corresponds to a reciprocal system [40]. This would be also the case of the electrical model by Stirnemann et al. [29] (Eq. 4) if the real part of the impedance Z_2 as given in Eq. (5) is negligible. Regarding the pump scattering matrix **S**, reciprocity brings about the same modulus for S_{11} and S_{22}, and the same argument for S_{12} and S_{21}, whereas the modulus of the determinant of **S** is equal to 1.

All this procedure to determine the transmission and the scattering matrices of pumps was conveniently implemented in a special calculation program developed with Delphi software. The resulting time of computation of the scattering matrix at 200 different frequencies for a pump with a seven blade impeller was less than 4 s with a conventional Intel Core i5 processor. This is about 40 times faster than with the acoustic model proposed in [36].

4. Effect of model parameters on predictions

The acoustic model was first put into practice on a reference pump with the main data shown in Table 2.

Table 2. Main input data for the reference pump:

Pump geometry:	
Diameter of suction port, d_S (mm)	100
Diameter of discharge port, d_D (mm)	65
Number of blades, z_B	7
Radius at impeller outlet, r_2 (mm)	105
Outlet angle relative to tangent, β_2 (deg)	26
Radius at tongue tip, r_3 (mm)	116
Width at impeller outlet, b_2 (mm)	16
Volute width, b_3 (mm)	40
Throttle cross-section, A_T (cm^2)	20
Length suction port to impeller eye, L_{SE} (mm)	90
Length throttle to discharge port, L_{TD} (mm)	240

Other model parameters:	
Angular position of first blade (trailing edge) relative to tongue, φ_1 (deg)	30
Number of segments for passages with variable cross-section, N	25
Peripheral expansion factor at impeller outlet, k_P	2
Sound speed, c (m/s)	1400

As described in Section 3, the sound field in the pump has to be computed twice, each under a different acoustic load, before determining the transmission matrix. An example of those computations is given in Fig. 8, which shows the modulus and phase of the pressure so obtained at four nodes, when the reference pump is subject to the acoustic load named *II* in Table 1. Calculations have covered a wide range of frequencies, from 0 to 400 Hz. The nodes selected are located at the suction and discharge ports of the pump (n_S and n_D), at the tongue region (n_{90}) and in the volute at the opposite side to the tongue (n_{50}). It is observed that, though differences between nodes increase with frequency, the three nodes from suction to tongue region exhibit a similar behavior, i.e. the acoustic pressure is relatively uniform in the chamber defined by the volute casing. Node n_D, however, shows a rather distinct trend, as corresponds to a position in a duct (the diffuser) at significant distance from the pump chamber.

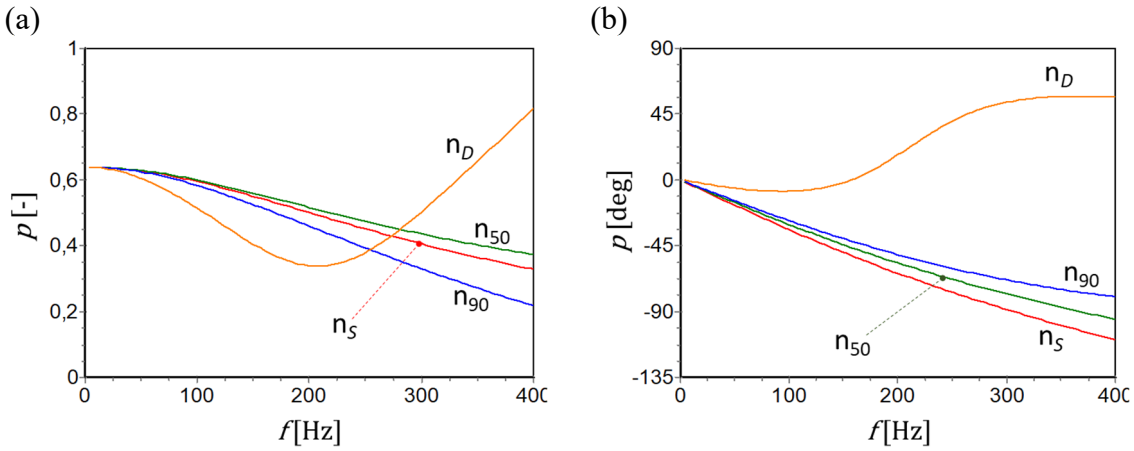

Fig. 8. Modulus (a) and phase (b) of the acoustic pressure at four nodes of the reference pump for the acoustic load *II* (Table 1). Nodes as in Fig. 7.

Appropriate processing according to Eq. 20 of the acoustic pressure and mass velocity at nodes n_S and n_D for the two acoustic loads of Table 1 results in the transmission matrix for the reference pump. This is shown in Fig. 9, as well as the predictions from Stirnemann's electrical analogy [29] as given by Eqs. (4-5) with $\mathrm{Re}(Z_2)$=0.

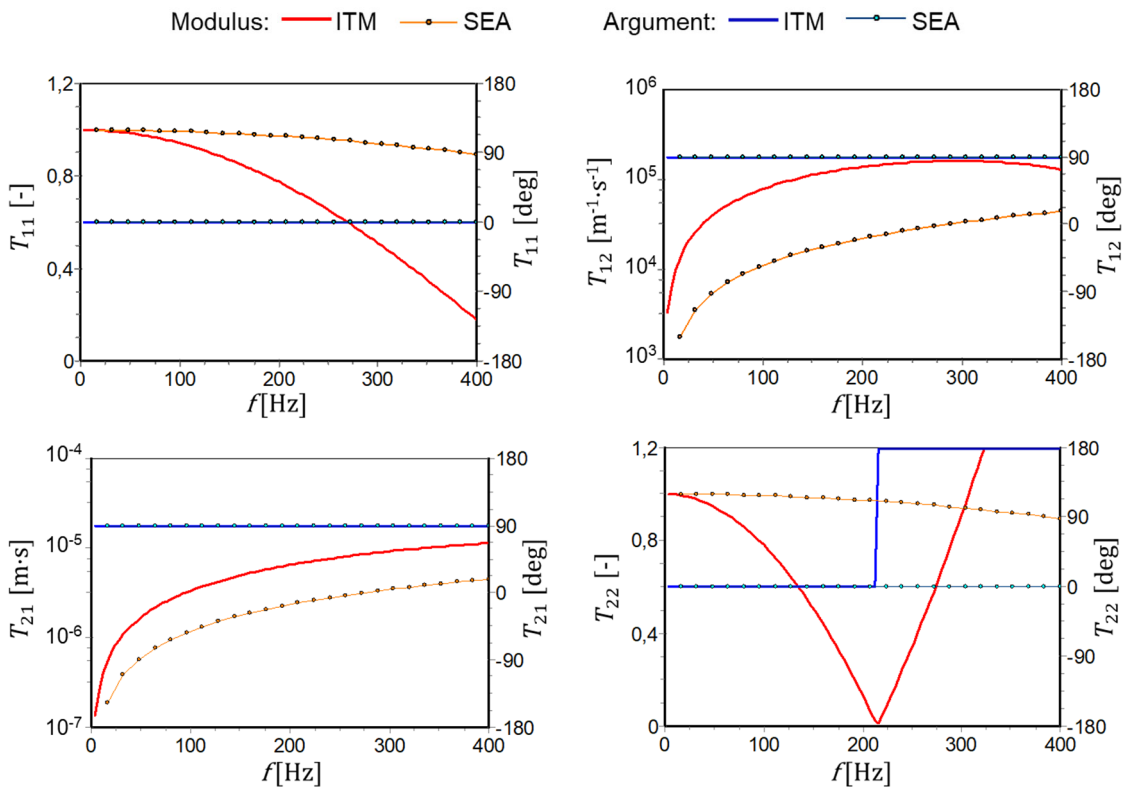

Fig. 9. Transmission matrix calculated for the reference pump. ITM= current internal transfer matrix model; SEA= Stirnemann's electrical analogy model, Eqs. (4-5).

The two models predict that elements T_{11} and T_{22} only have real part whereas T_{12} and T_{21} only have imaginary part, as expected. Also, increasing the frequency makes the modulus of T_{11} and T_{22} decay from unity with both models, but according to Eqs. (4-5) the slope of the decay is very smooth whereas the current transfer matrix model gives a quick reduction of magnitude, up to the point of reaching T_{22}=0 and then reversing phase and growing above 215 Hz. Besides, the magnitudes of T_{12} and T_{21} as predicted with Eqs. (4-5) are significantly lower than the values obtained from the transfer matrix model. All this suggests that, compared to the model now proposed, the values estimated with

Eq. (5) for the equivalent impedance and admittances are too low. This is in line with the observations by other researchers [30] and it is further discussed in next section.

Once the transmission matrix is known the scattering matrix can be obtained by using Eq. (21). A selection of results on the reference pump is given below to show the effect of some parameters of the acoustic model and also some pump parameters. Since no flow effects are considered in the model, the Helmholtz number is constant for a given pump geometry, and so the sound speed scales with frequency and pump size. In consequence, increasing the sound speed by, say, 5%, (or shrinking the pump lengths by 5%) results in a 5% stretching of each spectra data towards higher frequencies.

Among the acoustic parameters, the most influential one is the peripheral expansion factor k_P, which accounts for the effect of the abrupt change in cross-section at the outlet of the impeller channels (see section 2). The least possible value for k_P is 1, which actually means no peripheral expansion. As illustrated in Fig. 10 on element S_{11}, varying k_P from 1 to 2 and then to 3 accelerates the deviation of the variables when increasing frequency with respect to the values at 0 Hz. In particular, changing k_P from 1 to 2 gives a maximum relative change in the modulus of S_{11} of the order of 14% at about 200 Hz, whereas the argument reduces in 15°. Other model parameters have much less impact on the predictions. For instance, the number of segments N considered to estimate the transfer matrix of channels with variable cross-section (Fig. 5) proved to have virtually no influence on the results as far as it is higher than about 15. All the computations presented in this section and in the next one correspond to N=25.

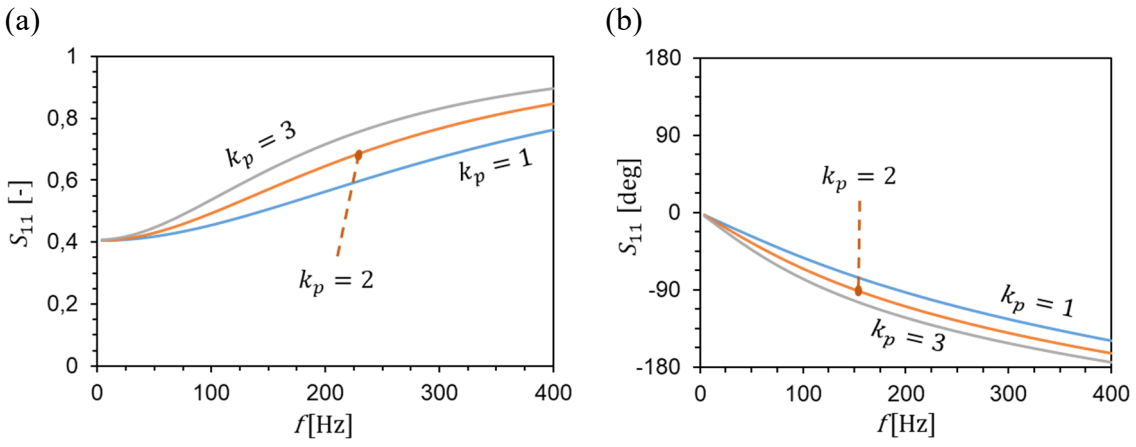

Fig. 10. Element S_{11} of the scattering matrix for the reference pump with peripheral expansion factors k_P=1, 2 and 3; (a) modulus; (b) argument.

With respect to the pump geometric parameters, the predictions of the scattering matrix show little dependence unless they are closely related to the global pump shape, i.e. to the pump specific speed. One example of parameters not dependent on specific speed is the angular position of the impeller, which is characterized by the angle φ_1 of the first blade (trailing edge) relative to tongue tip. In this case (Fig. 11), the maximum variation of the modulus of S_{11} for a range of φ_1 covering 360°/z_B (z_B=number of blades) is about 2% of the average value, whereas the phase varies in 2.5° as highest. This little variation is consistent with the measurements reported by Carta et al. [31] and supports dismissing the measure of that angle and even the rotation of the impeller for practical applications.

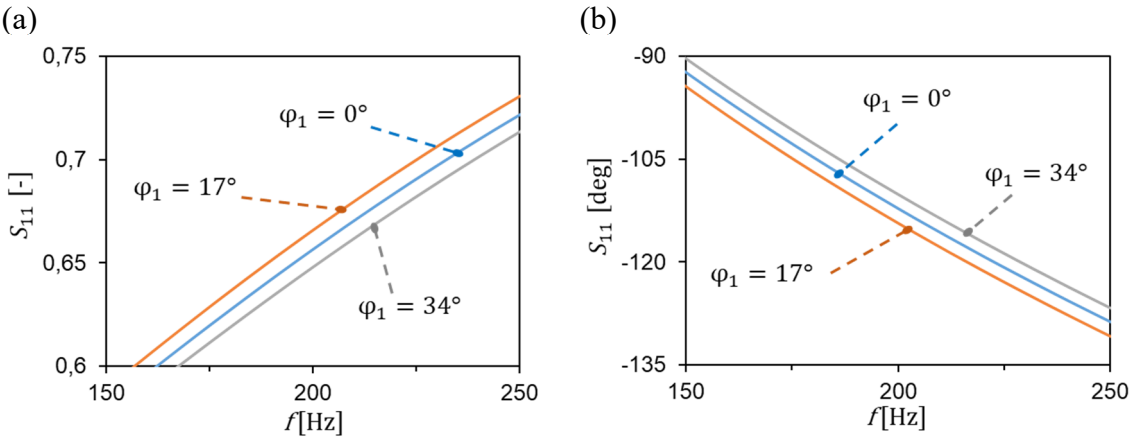

Fig. 11. Element S_{11} of the scattering matrix for the reference pump with impeller at angular positions φ_1= 0°, 17° and 34° (φ_1= angle of first blade relative to tongue); (a) modulus; (b) argument.

Fig. 12 shows the effect of cutting the impeller to a smaller outlet radius r_2 while keeping the same volute casing, which is a common practice of pump manufacturers to extend the performance range of the pumps. Again, its effect on the acoustic properties is small: a reduction of r_2 from 105 to 80 mm (24%) just leads to an increment of 3 % in the modulus of S_{11} and a reduction of 8° in the argument at 200 Hz.

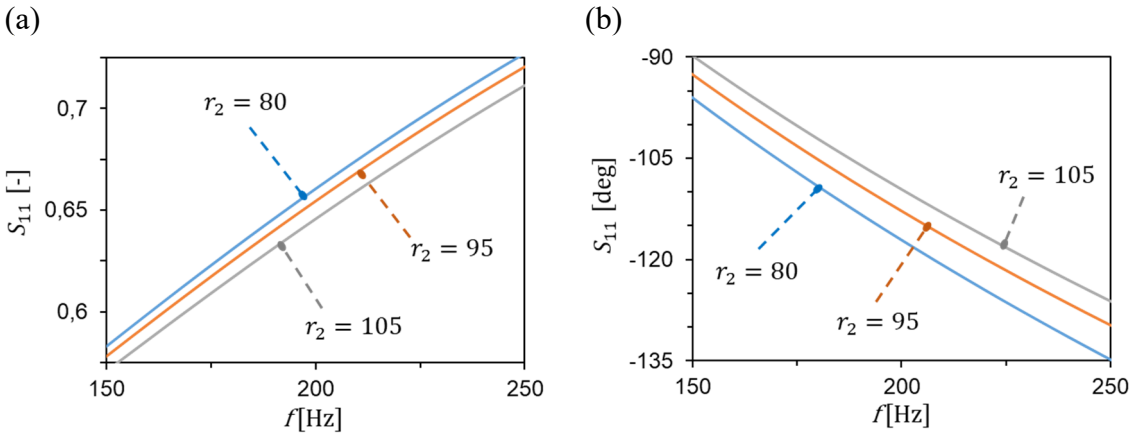

Fig. 12. Element S_{11} of the scattering matrix for the reference pump, with impeller outlet radius r_2 = 80, 95 and 105 mm; (a) modulus; (b) argument.

Another parameter with potential interest is the number of blades of the impeller, z_B, since it determines the number of nodes and internal transfer matrices involved in the pump acoustic model. However, Fig. 13 shows that varying z_B between 6 and 8 has little effect on the predicted modulus, and virtually no effect on the argument.

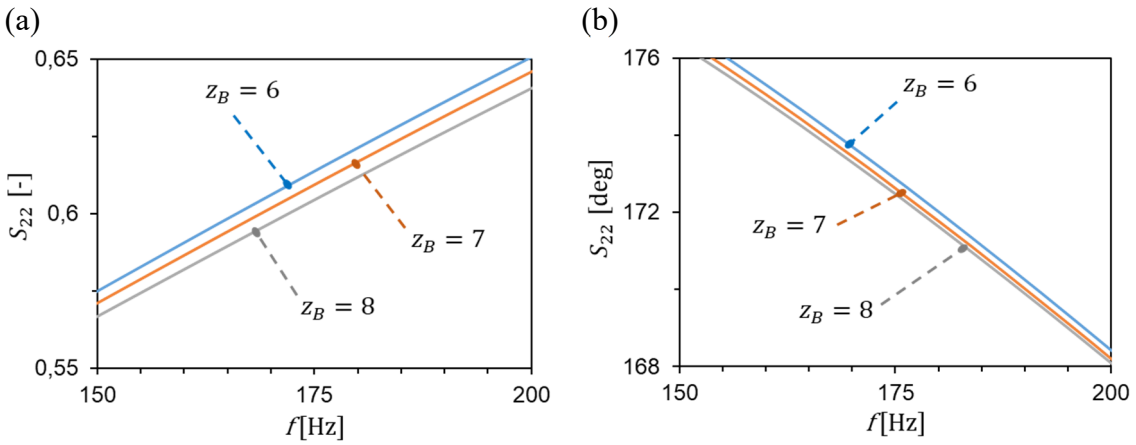

Fig. 13. Element S_{22} of the scattering matrix for the reference pump and impeller with z_B=6, 7 and 8 blades; (a) modulus; (b) argument.

5. Predictions vs experimental data

In order to evaluate the prediction capacity of the internal transfer matrix model, it was applied on a set of five pumps tested by Brümmer et al. [34, 35], who conducted laboratory measurements in standstill conditions to determine their scattering matrices.

The specific speed and main geometrical data reported (or easily derivable from the data reported) for those pumps are shown in Table 3. Pumps #1, #2 and #3 have the same inlet and outlet diameters, but their specific speed increases by a factor above 2. This indicates that the nominal flow-rate at a given rotational speed is in the same range for the three pumps, while the nominal head reduces to almost half. In consequence the size of the internal cross-section passages should be similar for the three pumps, whereas the external diameter of the impeller as well as the radial size of the casing reduce progressively from pump #1 to pump #3. Pump #4 has the same specific speed of pump #1 but its size is larger. Since the optimal geometry of fluid machinery depends basically on the specific speed, it is to be expected that pumps #1 and #4 are geometrically similar, with an approximate length scale factor of 100/65. Finally, pump #5 is identical to pump #1 except that the impeller was trimmed to an outside radius r_2 = 82.5 mm.

Table 3. Main data reported for the pumps tested by Brümmer et al. [34-35].

Pump designation	#1 (#5)	#2	#3	#4
Specific speed (non-dimensional), ω_S	0.46	0.70	0.99	0.46
Diameter of suction port, d_S (mm)	80	80	80	125
Diameter of discharge port, d_D (mm)	65	65	65	100
Number of blades, z_B	6	6	6	6
Radius at impeller outlet, r_2 (mm)	109.5 (82.5)	87.0	70.5	168.0
Radius at tongue tip, r_3 (mm)	117.6	96.6	78.8	180.5

Table 4. Additional geometric data used in the acoustic model.

Pump designation	#1 (#5)	#2	#3	#4
Width at impeller outlet, b_2 (mm)	7.5	9.5	13	12
Outlet blade angle relative to tangent, β_2 (deg)	32	35	38	22
Volute width, b_3 (mm)	50	45	40	85
Throttle cross-section, A_T (cm^2)	18	18	18	40
Length suction port to impeller eye, L_{SE} (mm)	80	80	80	150
Length throttle to discharge port, L_{TD} (mm)	200	135	100	300

The acoustic model operates with other non-reported input data, so they were estimated according to the pump specific speeds and the corresponding general shapes that manufactures use for each specific speed. Table 4 lists the main data assumed. Other model parameters were taken as constant for the five pump models, including: sound

speed c=1350 m/s (indicated in [34]), peripheral expansion factor k_P =2 and first blade angular position φ_1=30°.

Brümmer et al. [35] reported the scattering matrix data at seven specific frequencies between 150 Hz and 290 Hz for all the pumps but pump #4, for which data refers to 10 eleven frequencies between 95 and 190 Hz. As an example, Fig. 14 shows the experimental data corresponding to pump #4 together with the predictions derived from the new internal transfer matrix model (ITM) as well as from Stirnemann's electrical analogy (SEA) as formulated in Eqs. (4) and (5). Though the experimental data exhibit some dispersion, the ITM predictions can be considered in reasonable agreement with the measurements, especially regarding the argument. On the other hand, the trends of the parameters predicted with the SEA model for increasing frequency are similar to those of the experimental data, but the rate of variation of both modulus and argument with frequency is clearly too slow. This is consistent with the comparison in Fig. 9 between the modulus of the transmission matrix elements predicted from both models.

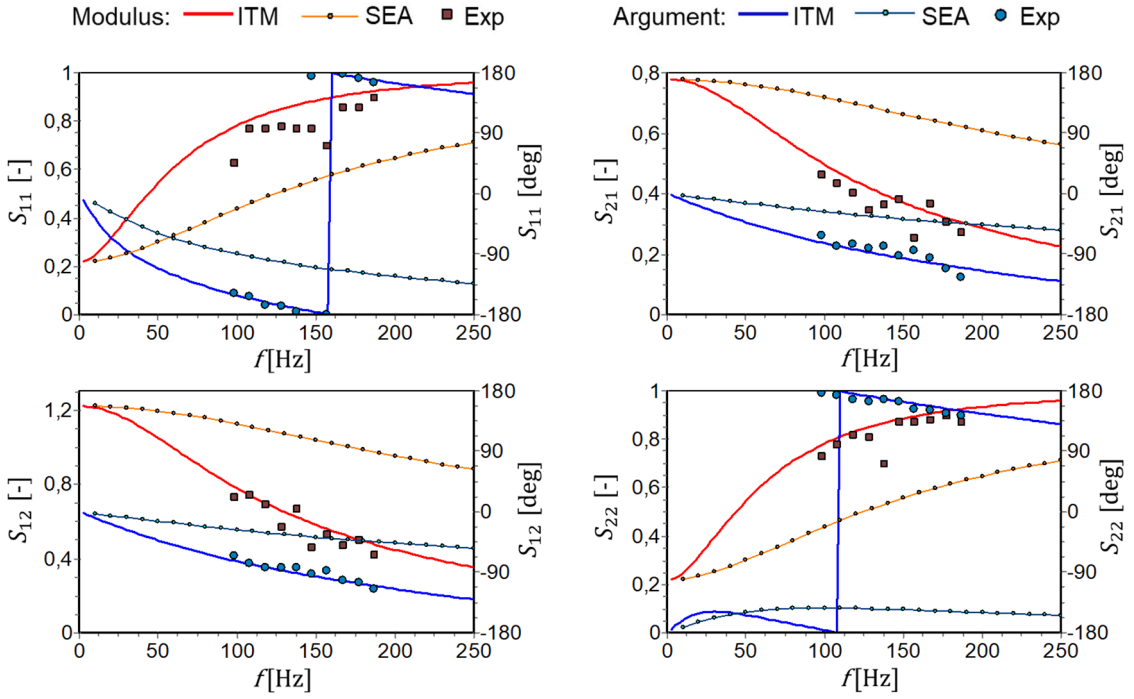

Fig. 14. Elements of the scattering matrix determined for Pump #4. ITM= internal transfer matrix model, SEA= Stirnemann's electrical analogy, Exp= data by Brümmer et al. [34, 35].

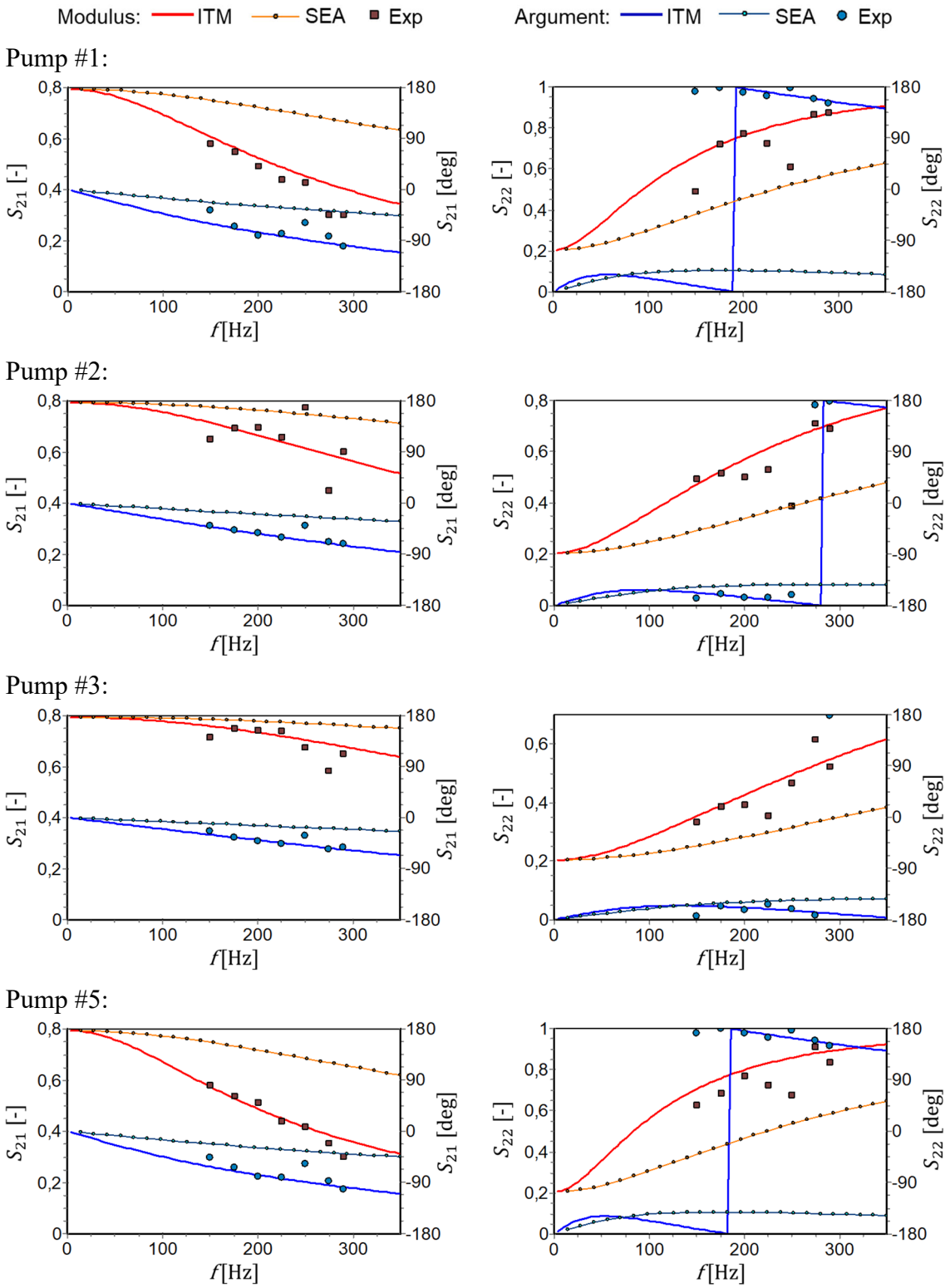

Fig. 15. Elements S_{21} and S_{22} of the scattering matrix determined for several pumps. ITM= internal transfer matrix model, SEA= Stirnemann's electrical analogy, Exp= data by Brümmer et al. [34, 35].

Reciprocity relationships are readily apparent when comparing the data for the four elements of the scattering matrix in Fig. 14. For instance, the predicted moduli of the

elements S_{11} and S_{22} at any given frequency are identical, and the corresponding experimental values are also very similar. The same happens regarding the argument of elements S_{12} and S_{21}.

Fig. 15 presents the experimental data and predictions corresponding to elements S_{21} and S_{22} for the rest of the pumps. Again, accordance with measurements can in general be considered fairly satisfactory with respect to the ITM predictions, whereas the SEA predictions diverge significantly from measurements when increasing the frequency.

Comparing the results for pumps #1, #2 and #3, it is readily observed that all of them present the same values at very low frequency, as correspond to machines that have input and output ports with the same cross-sections. On the other hand, the effect of frequency is qualitatively similar to that of an intermediate expansion chamber, whose volume changes from one pump to another. Among the three of them, pump #1 appears as the most sensitive one with respect to frequency, which is to be attributed to the larger size of its volute casing in the radial direction in order to allocate the impeller with the highest diameter. However the internal geometry of the pumps is indeed more complex than just having an expansion chamber with the volume of the pump casing. In fact, that volume is explicitly assumed in the SEA model (Eq. (5)), but the predictions are poorly correlated with the experimental data, as further discussed below.

The sensitivity to frequency still augments somewhat when considering pump #5 instead of pump #1, because the trimming of the impeller brings about a slight increment in the effective volume of the casing chamber. Nonetheless, the impact of impeller trimming on the pump scattering matrix is very small, as already observed for the reference pump in Fig. 12.

Finally, it is interesting to compare the data for pumps #1 (Fig. 15) and #4 (Fig. 14). As expected for geometrically similar pumps with different size, the respective curves of the scattering parameters appear to be shifted in the frequency scale by an amount approximately equal to the length scale factor. This has already been shown by Brümmer et al. [35] by using a Helmholtz number to scale the frequency axis.

An especial quality parameter was defined in order to quantify how close or far are predictions from the available experimental data, while taking into account that the experimental data can present some dispersion. The parameter used has been a variance ratio, VR, defined as the variance of the predictions relative to the experimental data (i.e., the mean squared error) divided by the variance of the experimental data relative to their average value. In particular, the variance ratio VR that corresponds to any of the four elements s of the pump scattering matrix has been calculated by means of Eq. (22):

$$\mathrm{VR}(s) = \frac{\sum_{i=1}^{n}[(s_{PRi} - s_{ERi})^2 + (s_{PIi} - s_{EIi})^2]}{\sum_{i=1}^{n}[(s_{ERi} - \overline{s_{ER}})^2 + (s_{EIi} - \overline{s_{EI}})^2]} \tag{22}$$

where s is any of the four elements of the pump scattering matrix, n is the number of experimental data available, subscripts E and P denote experimental or predicted values at the same frequency and subscripts R and I denote real or imaginary components. According to the definition, this variance ratio parameter can only take positive values, the closer VR to zero, the better the predictions.

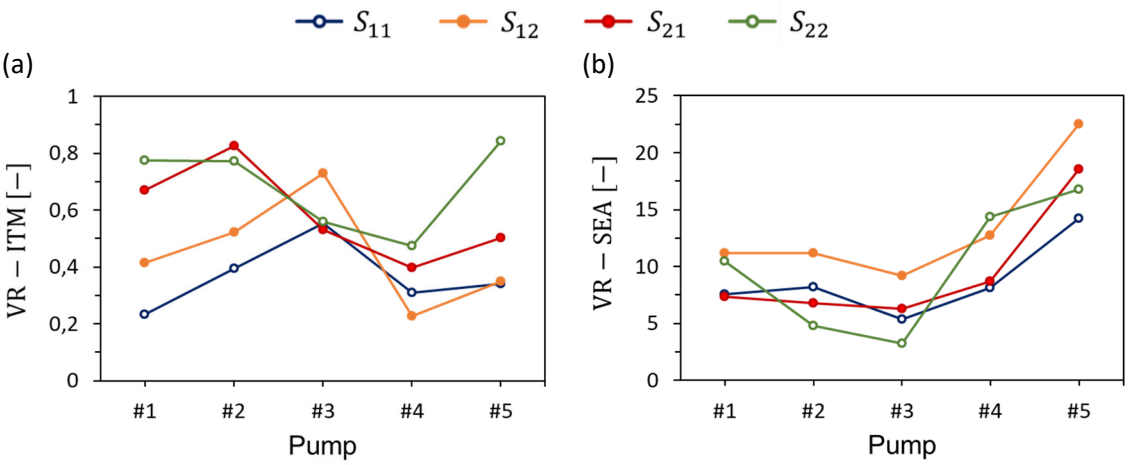

Fig. 16. Variance ratio parameter for the elements of the scattering matrix of five pumps. Predictions from (a) internal transfer matrix model and (b) Stirnemann's electrical analogy.

Fig. 16 shows the VR parameters so obtained for each element of the scattering matrix and for the five pumps tested. The predictions derived from the new internal transfer matrix model (ITM) give VR parameters always below 0.85, the lowest one usually associated to the suction reflection element S_{11}. The average VR for each pump lies in the range 0.5-0.6 except for pump #4, which takes a somewhat lower value, about 0.35,

possibly because of having more experimental data available for that pump. Therefore, it may be concluded that the ITM model performs similarly and reasonably well regardless the pump specific speed, i.e., it does not really show a shape dependence. And the results for pump #4 suggest that there is no size dependence either. All that leads to conclude that the new ITM model can be considered adequate for its future use in a tool to explore the properties of internal sound sources in pumps, following the approach of references [13, 36].

In comparison, the VR values corresponding to the predictions from Stirnemann´s electrical analogy (SEA) with Eqs. (4-5) are at least one order of magnitude larger. Predictions are especially poor for pump #4 and even worse for pump #5. Considering that discrepancies between measurements and SEA predictions arise because the latter change too little with frequency (as seen in Figs. 14 and 15), it may be concluded that Eq. (5) systematically underpredicts the equivalent impedance and admittances of the pump. That becomes more evident when the volume of the volute casing increases in the radial direction with respect to the impeller, either because the entire pump is bigger (pump #4) or because the impeller is shorter (pump #5). The latter is also supported by the slight reduction of the average VR that exhibits Fig. 16(b) when going from pump #1 to #2 and #3, i.e., when increasing the specific speed.

6. Conclusions

In order to simulate the internal sound field in centrifugal pumps at low frequency (plane wave mode), a new model has been developed based on a selection of internal nodes connected by means of local transfer matrices, which are dependent on the pump geometry. In general, these local transfer matrices correspond to passages with variable cross-section, and so they were estimated by means of segmentation with the matrizant approach. As a first application, the proposed internal transfer matrix model has been used in a procedure to estimate either the global transmission matrix or the scattering matrix of a given pump as a function of frequency. Sensitivity tests conducted on a reference pump show that, in general, the results are little affected by changes in the acoustic parameters except the periphery expansion factor, which characterizes the abrupt change in cross-section for the acoustic waves in the transition region between impeller

channels and volute. Besides, the predictions happen to be little dependent on geometry parameters that are not closely related to the pump specific speed or size.

The predictions of the new internal transfer matrix model, as well as from Stirnemann's classical model [29] based on an electrical analogy, have been contrasted against the experimental data reported by Lehr et al. [34] and Brümmel et al. [35] on the scattering matrices for five pumps with different specific speeds and features.

The results from Stirnemann's electrical analogy show trends of frequency dependence that are qualitatively in line with the experimental data, but predictions diverge quickly from measurements for increasing frequencies. It has been inferred that the values of the equivalent impedance and admittances considered in that model are systematically under-estimated, especially for pumps with large volute casing.

On the contrary, the new internal transfer matrix model has given predictions of the four elements of the scattering matrix, both in modulus and phase, that are in reasonable quantitative agreement with the experimental data for the five pumps tested. According to a variance ratio parameter determined for each case, the degree of goodness of the predictions is similar for all the pumps tested regardless the specific speed.

All this supports the possible future use of this new model complemented with internal acoustic sources in order to characterize pump noise excitation mechanisms at low frequency, such as the excitation associated with blade passing in front of the volute tongue. First, that will require to modify the pump acoustic model so that it can incorporate additional nodes that allocate sound sources with arbitrary properties for a given frequency (magnitude, phase and position). Then the acoustic model is to be implemented in an iterative approach that contrasts predictions against experimental data, analogous to that of Parrondo et al. [36] and Keller et al. [13]. This is intended as the next step of this research.

Acknowledgements

The authors acknowledge the financial support received from the Principado de Asturias (Spain) under grant FC-GRUPIN-IDI/2018/000205, as well as the grant awarded to Mr. Guidong Li by the China Scholarship Council.

References

[1] Bolleter U. Interaction of Pumps and Piping Systems with Regard to Pressure Pulsations. In: Proc 1st Int. Symp. on Pump Noise and Vibration. Centre Technique des Industries Méchaniques; 1993, p. 3-10.

[2] Rzentkowski G, Zbroja S. Experimental characterization of centrifugal pumps as an acoustic source at the blade-passing frequency. J Fluids Struct 2000;14:529–58. https://doi.org/10.1006/jfls.1999.0280.

[3] Barzdaitis V, Mažeika P, Vasylius M, Kartašovas V, Tadžijevas A. Investigation of pressure pulsations in centrifugal pump system. J Vibroengineering 2016;18:1849–60. https://doi.org/10.21595/jve.2016.15883.

[4] Okasha A, Elnady T, Åbom M. Analysis of pipeline networks using two-ports. Appl Acoust 2016;109:44–53. https://doi.org/10.1016/j.apacoust.2016.02.008.

[5] Guelich JF, Bolleter U. Pressure pulsations in centrifugal pumps. J Vib Acoust Trans ASME 1992;114:272–9. https://doi.org/10.1115/1.2930257.

[6] Si Q, Ali A, Yuan J, Fall I, Muhammad Yasin F. Flow-Induced Noises in a Centrifugal Pump: A Review. Sci Adv Mater 2019;11:909–24. https://doi.org/10.1166/sam.2019.3617.

[7] Guo C, Gao M, He S. A review of the flow-induced noise study for centrifugal pumps. Appl Sci 2020;10. https://doi.org/10.3390/app10031022.

[8] Wu D, Ren Y, Mou J, Gu Y. Investigation of the correlation between noise & vibration characteristics and unsteady flow in a circulator pump. J Mech Sci Technol 2017;31:2155–66. https://doi.org/10.1007/s12206-017-0411-y.

[9] Zhang N, Liu X, Gao B, Xia B. DDES analysis of the unsteady wake flow and its evolution of a centrifugal pump. Renew Energy 2019;141:570–82. https://doi.org/10.1016/j.renene.2019.04.023.

[10] Parrondo-Gayo JL, González-Pérez J, Fernández-Francos J. The effect of the operating point on the pressure fluctuations at the blade passage frequency in the volute of a centrifugal pump. J Fluids Eng Trans ASME 2002;124:784–90. https://doi.org/10.1115/1.1493814.

[11] Cheng X, Wang P, Zhang S. Correlation Research between Turbulent Pressure Pulsation and Internal Sound Field Characteristics of Centrifugal Pump. J Therm Sci 2020. https://doi.org/10.1007/s11630-020-1253-y.

[12] Zhang N, Jiang J, Gao B, Liu X. DDES analysis of unsteady flow evolution and pressure pulsation at off-design condition of a centrifugal pump. Renew Energy 2020;153:193–204. https://doi.org/10.1016/j.renene.2020.02.015.

[13] Keller J, Parrondo J, Barrio R, Fernández J, Blanco E. Effects of the pump-circuit acoustic coupling on the blade-passing frequency perturbations. Appl Acoust 2014;76:150–6. https://doi.org/10.1016/j.apacoust.2013.06.009.

[14] Hayashi I, Kaneko S. Pressure pulsations in piping system excited by a centrifugal turbomachinery taking the damping characteristics into consideration. J Fluids Struct 2014;45:216–34. https://doi.org/10.1016/j.jfluidstructs.2013.11.012.

[15] Rzentkowski G, Zbroja S. Acoustic characterization of a CANDU primary heat transport pump at the blade-passing frequency. Nucl Eng Des 2000;196:63–80. https://doi.org/10.1016/S0029-5493(99)00235-6.

[16] Barrio R, Keller J, Fernández J, Blanco E, Parrondo J. Prediction of pump-circuit interactions by computational fluid dynamics calculations coupled with a one-dimensional acoustic model. Proc Inst Mech Eng Part C J Mech Eng Sci 2015;229:1172–81. https://doi.org/10.1177/0954406214542640.

[17] Yang J, Yuan S, Yuan J, Si Q, Pei J. Numerical and experimental study on flow-induced noise at blade-passing frequency in centrifugal pumps. Chinese J Mech Eng (English Ed 2014;27:606–14. https://doi.org/10.3901/CJME.2014.03.606.

[18] Liu HL, Dai HW, Ding J, Tan MG, Wang Y, Huang HQ. Numerical and experimental studies of hydraulic noise induced by surface dipole sources in a centrifugal pump. J Hydrodyn 2016;28:43–51. https://doi.org/10.1016/S1001-6058(16)60606-6.

[19] Chen J, He Y, Gui L, Wang C, Chen L, Li Y. Aerodynamic noise prediction of a centrifugal fan considering the volute effect using IBEM. Appl Acoust 2018;132:182–90. https://doi.org/10.1016/j.apacoust.2017.10.015.

[20] Si Q, Shen C, He X, Li H, Huang K, Yuan J. Numerical and experimental study on the flow-induced noise characteristics of high-speed centrifugal pumps. Appl Sci 2020;10. https://doi.org/10.3390/app10093105.

[21] Liu H, Ding J, Dai H, Tan M, Tang X. Numerical research on hydraulically generated vibration and noise of a centrifugal pump volute with impeller outlet width variation. Math Probl Eng 2014;2014. https://doi.org/10.1155/2014/620389.

[22] Luan HX, Chen QG, Weng LY, Luan YZ, Li J. Numerical computation of the flow noise for the centrifugal pump with considering the impeller outlet width. J Vibroengineering 2016;18:2601–12. https://doi.org/10.21595/jve.2016.16656.

[23] Guo C, Gao M, Wang J, Shi Y, He S. The effect of blade outlet angle on the acoustic field distribution characteristics of a centrifugal pump based on Powell vortex sound theory. Appl Acoust 2019;155:297–308. https://doi.org/10.1016/j.apacoust.2019.05.031.

[24] Guo C, Gao M, Wang J. Acoustic distribution study inside centrifugal pump impeller under different blade outlet angles using the Powell vortex sound theory. Proc Inst Mech Eng Part C J Mech Eng Sci 2020;234:2595–609. https://doi.org/10.1177/0954406220908732.

[25] Yu-qin W, Ze-wen D. Influence of blade number on flow-induced noise of centrifugal pump based on CFD/CA. Vacuum 2020;172. https://doi.org/10.1016/j.vacuum.2019.109058.

[26] Guo R, Li R, Zhang R, Han W. The action mechanism of rotor-stator interaction on hydraulic and hydroacoustic characteristics of a jet centrifugal pump impeller and performance improvement. Water (Switzerland) 2020;12. https://doi.org/10.3390/w12020465.

[27] Lavrentjev J, Åbom M, Bodén H. A measurement method for determining the source data of acoustic two-port sources. J Sound Vib 1995;183:517–31. https://doi.org/10.1006/jsvi.1995.0268.

[28] Carta F, Bolpaire S, Charley J, Caignaert G. Hydroacoustic Source Characterisation of Centrifugal Pumps. Int J Acoust Vib 2002;7:110-4. https://doi.org/10.20855/ijav.2002.7.2108.

[29] Stirnemann A, Eberl J, Bolleter U, Pace S. Experimental determination of the dynamic transfer matrix for a pump. J Fluids Eng Trans ASME 1987;109:218–25. https://doi.org/10.1115/1.3242651.

[30] Bardeleben MJR, Weaver DS. Estimation of the acoustic scattering matrix for a centrifugal pump. ASME Int. Mech. Eng. Congr. Expo. Proc., 2002, p. 809–19. https://doi.org/10.1115/IMECE2002-33354.

[31] Carta F, Charley J, Caignaert G. Transfer Matrices of Single Volute Centrifugal Pumps. Int J Acoust Vib 2000;5: 159-66. https://doi.org/10.20855/ijav.2000.5.462.

[32] Han Y, Smith BAW, Luloff B V. Use of redundant sensors to determine the acoustic transfer matrix of a pump. Am. Soc. Mech. Eng. Press. Vessel. Pip. Div. PVP, vol. 465, 2003, p. 169–78. https://doi.org/10.1115/PVP2003-2087.

[33] Villouvier V. Modelling of the hydroacoustic transfers through a centrifugal pump. EURONOISE 2006 - 6th Eur. Conf. Noise Control Adv. Solut. Noise Control, 2006.

[34] Lehr C, Linkamp A, Aurich D, Brümmer A. Simulations and experimental investigations on the acoustic characterization of centrifugal pumps of different specific speed. Int J Turbomachinery, Propuls Power 2019;4. https://doi.org/10.3390/ijtpp4030016.

[35] Brümmer A, Lehr C, Linkamp A. Entwicklung von Grundlagen für instationär betriebene hydraulische Pumpensysteme in flexiblen Kraftwerken; Teilprojekt TP2, Arbeitspaket AP4: Druckpulsationen in instationär betriebenen hydraulischen Systemen, Technical Report, TU Dortmund, 2019. https://doi.org/10.2314/kxp:1667387111.

[36] Parrondo J, Pérez J, Barrio R, González J. A simple acoustic model to characterize the internal low frequency sound field in centrifugal pumps. Appl Acoust 2011;72:59–64. https://doi.org/10.1016/j.apacoust.2010.08.005.

[37] Mimani A, Munjal ML. Transverse plane-wave analysis of short elliptical end-chamber and expansion-chamber mufflers. Int. J. Acoust. Vib., vol. 15, 2010, p. 24–38. https://doi.org/10.20855/ijav.2010.15.1256.

[38] Munjal ML. Theory of Acoustic Filters. In: Acoustics of Ducts and Mufflers 2nd Edition. Wiley; 2014.

[39] Burden RL, Faires JD. Numerical Analysis 9th Edition. 2011. https://doi.org/10.1017/CBO9781107415324.004.

[40] Brennen C. Unsteady Flow in Hydraulic Systems. In Hydrodynamics of Pumps, 2011. https://doi.org/10.1017/cbo9780511976728.011.